Journal of Magnetism and Magnetic Materials 384 (2015) 255–265

Contents lists available at ScienceDirect

Journal of Magnetism and Magnetic Materials

journal homepage: www.elsevier.com/locate/jmmm

Magneto-optical activity of *f–f* transitions in $ErFe_3(BO_3)_4$ and $ErAl_3(BO_3)_4$ single crystals

A.V. Malakhovskii [a,*], A.L. Sukhachev [a], V.V. Sokolov [b], T.V. Kutsak [b], V.S. Bondarev [a,b], I.A. Gudim [a]

[a] L.V. Kirensky Institute of Physics, Siberian Branch, Russian Academy of Sciences, 660036 Krasnoyarsk, Russian Federation
[b] Siberian Federal University, Krasnoyarsk 660041, Russian Federation

ARTICLE INFO

Article history:
Received 5 November 2014
Received in revised form
19 February 2015
Accepted 23 February 2015
Available online 24 February 2015

Keywords:
Magnetic circular dichroism
Natural circular dichroism
Rare earth ferroborates
Rare earth alumoborates
Electronic structure

ABSTRACT

Absorption, magnetic circular dichroism and natural circular dichroism spectra of $ErFe_3(BO_3)_4$ and $ErAl_3(BO_3)_4$ single crystals were measured as a function of temperature in the range of 90–293 K. It was found out that magneto-optical activity of the same *f–f* transitions in the studied crystals substantially differed and their temperature dependences did not follow the Curie–Weiss law in contrast to the properties of allowed transitions. The observed phenomena were accounted for by the nature of *f–f* transitions allowance. Properties of the transition $^4I_{15/2} \rightarrow {}^4S_{3/2}$ were studied in detail. In particular, the Zeeman splitting and the natural optical activity of the absorption lines composed of the transition were determined. The vibronic line with the very large natural optical activity was revealed and identified. Two nonequivalent Er^{3+} ion positions with the opposite chirality were found out in one of the excited states. Polarization properties of the $^4I_{15/2} \rightarrow {}^4S_{3/2}$ transition in the $ErFe_3(BO_3)_4$ crystal have shown that the local symmetry of Er^{3+} ion in this crystal in the range of 90–293 K is lower than the D_3 one. From the heat capacity measurements it was revealed, that the first order structural phase transition to lower symmetry occurred in $ErFe_3(BO_3)_4$ at 433–439 K.

1. Introduction

Borates of the $RM_3(BO_3)_4$ type (R–Y or rare earth (RE) metal, M–Al, Ga, Cr, Fe, Sc) have huntite-like structure with the trigonal space group *R32* (D_3^7) in the high temperature phase. Er^{3+} is a widely-spread active ion used in solid state lasers. For example, laser generation was obtained in the $YAl_3(BO_3)_4$ crystal with an admixture of Er^{3+} ion [1–3]). The huntite-like structure has no center of inversion. Therefore, crystals of this type can be used also as nonlinear active media [4, 5]. Erbium-containing crystals demonstrate up-conversion luminescence due to the energy transfer between exited ions of the same kind [6–8]. Spectroscopic properties of the $ErAl_3(BO_3)_4$ crystal were studied in Ref. [9] and those of the $ErFe_3(BO_3)_4$ crystal in Ref. [10]. Some feroborates ($ErFe_3(BO_3)_4$, in particular) have structural phase transition to lower symmetry $P3_121$ (D_3^4). At this transition, the local symmetry of RE ion decreases from D_3 to C_2 one. Structure of $ErAl_3(BO_3)_4$ and $ErFe_3(BO_3)_4$ crystals was studied in Refs. [9] and [10], respectively. Both crystals have highly anisotropic magnetic properties [11–13], and their paramagnetic magnetization substantially deviates from the Curie–Weiss law.

Considerable part of ferroborates of the $RFe_3(BO_3)_4$ type refers to multiferroics [14], i. e., they possess magnetic and electric polarizations simultaneously. However, electric polarization in the $ErFe_3(BO_3)_4$ crystal is very small [14]. At the same time, the $ErAl_3(BO_3)_4$ crystal demonstrates rather large electric polarization in magnetic field [11]. All RE ferroborates transfer from the paramagnetic to magnetically ordered state at temperatures below 30–40 K. In particular, the $ErFe_3(BO_3)_4$ crystal becomes easy plane antiferromagnetic at $T_N = 38$ K [15–17].

There are many works devoted to study of magnetic circular dichroism (MCD) of *f–f* transitions in solids. We will mention only those devoted to the Er^{3+} ion in different compounds. In particular, the MCD was studied in erbium containing glasses [18–21] and in crystals [22, 23]. The MCD gives additional information about electronic states such as sign and value of the Zeeman splitting, when it is not seen directly [24], and helps to identify the initial and final states of transitions. The MCD of the parity forbidden *f–f* transitions gives also information about nature of the *f–f* transitions allowance [24]. All these properties will be used in the present work. More particularly, the MCD is measured only at one or several temperatures, and the MCD spectra are decomposed on the diamagnetic and paramagnetic parts, but the nature of the *f–f* transitions MCD is not analyzed. In the present investigation, the

* Corresponding Author. Fax: +7 391 2438923.
E-mail address: malakha@iph.krasn.ru (A.V. Malakhovskii).

http://dx.doi.org/10.1016/j.jmmm.2015.02.051
0304-8853/

absolute values and temperature dependences of the integral paramagnetic magneto-optical activity (MOA) of *f–f* transitions in the $ErFe_3(BO_3)_4$ and $ErAl_3(BO_3)_4$ single crystals are measured and nature of the observations is analyzed and accounted for. Comparative study of the magneto-optical properties of crystals with the very close structure, fulfilled in the present work, is of the special interest from the viewpoint of nature of the *f–f* transitions MOA.

Since the local symmetry of the Er^{3+} ion in the studied crystals has no center of inversion, the natural circular dichroism (NCD) can exist. In the $ErAl_3(BO_3)_4$ it was really observed and studied. The NCD is widely used for the study of organic compounds. However, there are not so many works devoted to the NCD in inorganic crystals (e.g., [25–29]), and in the Er containing crystals, in particular [26, 27]. Temperature dependences of the NCD give the information about transformations of the local environment of the active ion in its excited state.

2. Experimental details

Single crystals of $ErAl_3(BO_3)_4$ were grown at small overcooling on seeds from the flux 90% mass ($Bi_2Mo_3O_{12}+2B_2O_3+0.5Li_2MoO_4$)+10% mass $ErAl_3(BO_3)_4$. This flux has saturation temperature $T_{sat}=960$ °C. Details of the growth procedure have been described in Ref. [30]. Earlier the same crystal was grown from another flux [31]. $ErFe_3(BO_3)_4$ single crystals were grown from the melt solution as described in Ref. [13]. As grown-up crystals had the size of 5x5x7 mm^3.

As mentioned above, the crystals belong to the trigonal symmetry. The lattice constants of the $ErAl_3(BO_3)_4$ are [9]: $a=9.2833$ (7) Å, $c=7.2234(6)$ Å and those of $ErFe_3(BO_3)_4$ [10]: $a=9.566(4)$ Å, $c=7.591(3)$ Å. The unit cell contains three formula units. Trivalent RE ions occupy positions of only one type. They are located at the center of trigonal prisms of the D_3 symmetry made up of six crystallographically equivalent oxygen ions [32]. The FeO_6 and AlO_6 octahedrons share edges in such a way that they form helicoidal chains, which run parallel to the C_3 axis and are mutually independent. All Fe and Al ions occupy C_2-symmetry positions in the crystals.

The absorption spectra were measured by the two beam technique, using an automated spectrophotometer designed on the basis of the diffraction monochromator MDR-2. They were obtained with the light propagating normally to the C_3 axis of the crystal for the light electric vector $\vec{E}$ parallel (π spectrum) and perpendicular (σ spectrum) to the C_3 axis, and for the light propagating along the C_3 axis (α spectrum). Optical slit width (spectral resolution) was 0.2 nm in the region of 300–600 nm and 0.4 nm in the region of 600–1100 nm.

The MCD and NCD spectra were recorded with the light propagating along the C_3 axis of the crystals. The magnetic field of 5 kOe was also directed along the C_3 axis. The circular dichroism was measured using the modulation of the light wave polarization with the piezoelectric modulator (details see in Ref. [33]). The MCD was obtained as a half difference of the circular dichroisms at opposite magnetic fields and NCD was obtained as a half sum of these values. The sensitivity in measuring of the circular dichroism was 10^{-4}, and the spectral resolution was the same as that at the absorption spectra measuring. The sample was put in a nitrogen gas flow cryostat. Accuracy of the temperature measuring was ~1 K. Thickness of the $ErAl_3(BO_3)_4$ samples was 0.3 mm and that of the $ErFe_3(BO_3)_4$ samples was 0.2 mm.

The temperature dependence of the heat capacity $\Delta C_p(T)$ of the $ErFe_3(BO_3)_4$ crystal was measured on a DSM-10Ma differential scanning microcalorimeter (DSM) in the temperature range from 100 K to 520 K. The experiments were performed in a helium atmosphere on a sample with a weight of 69 mg in the dynamic mode with heating and cooling rates of 16 K/min. The sample was packed in an aluminum container without any heat conducting greases. The average deviation of the experimental data from the smoothed curve $\Delta C_p(T)$ does not exceed 1%. The error in the determination of the integral characteristics (enthalpy and entropy) was equal to ~10%.

3. Results and discussion

The absorption, MCD and NCD spectra of the $ErAl_3(BO_3)_4$ crystal were measured in the spectral range of 9600–29,000 cm^{-1} (Figs. 1–3). The identification of *f–f* absorption bands was made according to Kaminskii [34]. The absorption and MCD spectra of the $ErFe_3(BO_3)_4$ crystal were measured in the range of 9600–21,700 cm^{-1}. The NCD in the $ErFe_3(BO_3)_4$ was on the level of noise. This means that the number of the opposite inverse twins in the crystal is approximately equal. The absorption spectra of the studied crystals in σ and α polarizations coincide within the limit of the experimental error, that testifies to electric dipole character of the transitions. The absorption spectrum of the $ErFe_3(BO_3)_4$ crystal (Fig. 4) consists of narrow bands corresponding to *f–f* transitions in Er^{3+} ions and of wide bands due to *d–d* transitions in Fe^{3+} ions ($^6A_1 \rightarrow {}^4T_1$ and $^6A_1 \rightarrow {}^4T_2$ in the cubic crystal field notation). It is known [35] that at $E \sim 22{,}900$ cm^{-1} there is a comparatively strong *d–d* transition $^6A_1 \rightarrow {}^4A_1{}^4E$ and at $E \sim 25{,}000$ cm^{-1} the edge of the strong absorption occurs, which is due to the interatomic Fe–Fe (Mott–Hubbard) transitions. These transitions were too strong to be measured in our sample and they overlapped the *f–f* transitions. The *d–d* absorption bands were approximated by the Gauss functions and subtracted from the total spectrum. As a result, the *f–f* absorption spectrum was obtained. It appeared that the MCD of the *d–d* transitions was too small to be observed (Fig. 5). All enumerated spectra were measured and treated as a function of temperature in the interval of 90–293 K.

3.1. Paramagnetic magneto-optical activity of f–f transitions

The MCD of a line split on two components by the magnetic field directed along the light propagation can be given by the equation:

$$\Delta k = k_{m+}\phi(\omega, \omega_0 + \Delta\omega_0) - k_{m-}\phi(\omega, \omega_0 - \Delta\omega_0) \quad (1)$$

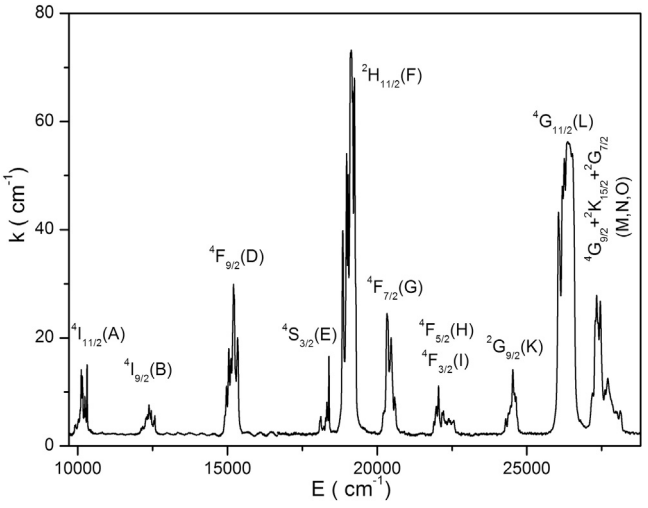

Fig. 1. Absorption spectrum of $ErAl_3(BO_3)_4$ at room temperature.

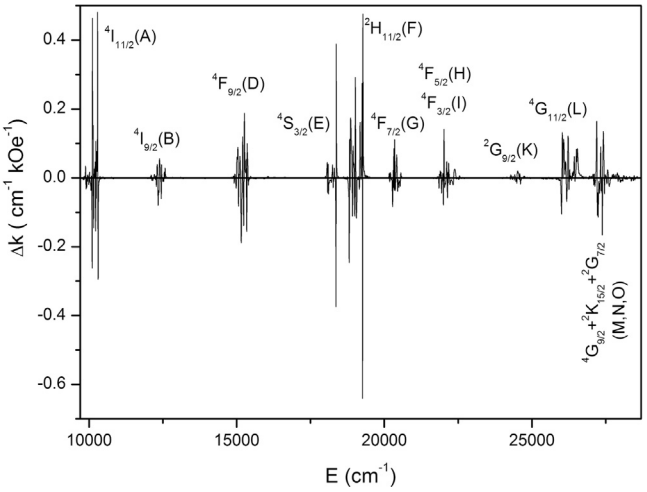

Fig. 2. MCD spectrum of $ErAl_3(BO_3)_4$ at room temperature.

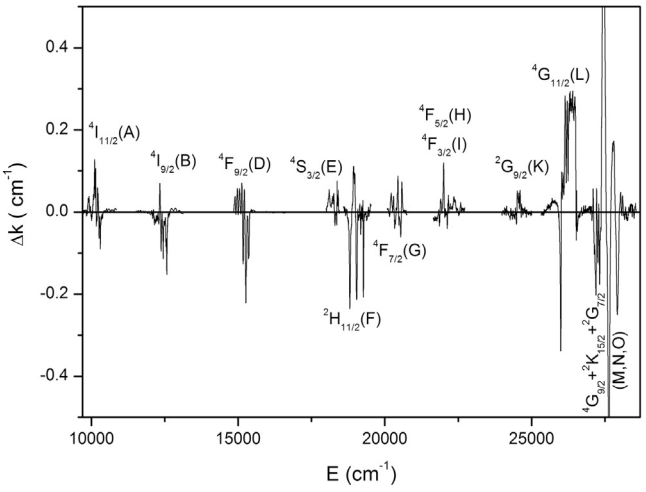

Fig. 3. NCD spectrum of $ErAl_3(BO_3)_4$ at room temperature.

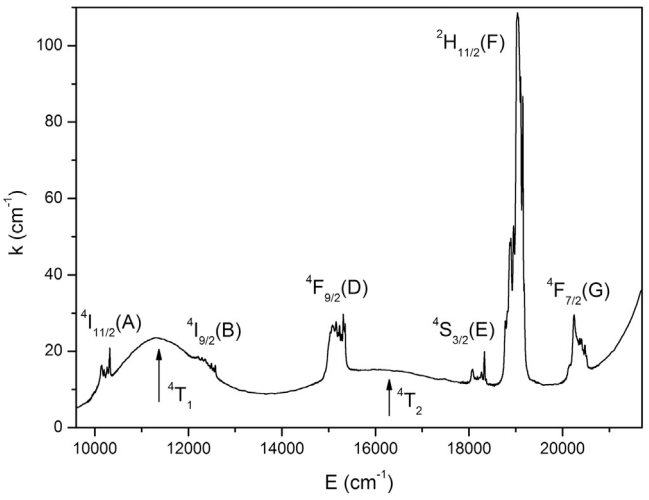

Fig. 4. Absorption spectrum of $ErFe_3(BO_3)_4$ at room temperature.

Here k_{m+} and k_{m-} are amplitudes of (+) and (−) circularly polarized lines; φ are form functions of (+) and (−) polarized lines. If the Zeeman splitting $\Delta\omega_0$ is much less than the line width then, after developing of the φ-functions as series in $\Delta\omega_0$, it is obtained:

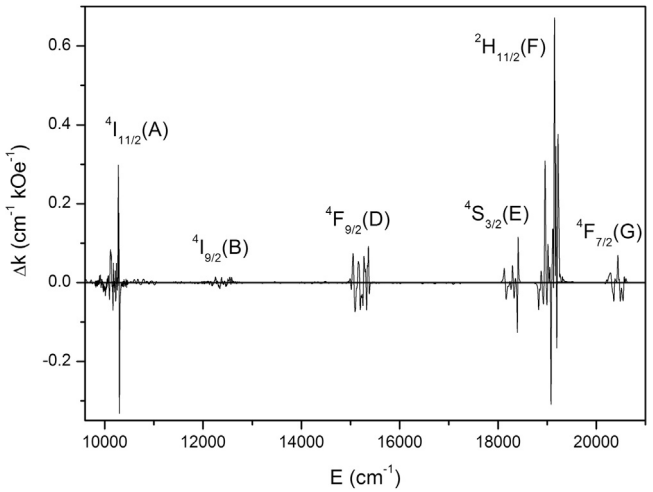

Fig. 5. MCD spectrum of $ErFe_3(BO_3)_4$ at room temperature.

$$\Delta k = k_m c\phi(\omega, \omega_0) + k_m \Delta\omega_0 \partial\phi(\omega, \omega_0)/\partial\omega_0 \quad (2)$$

Here $k_m = k_{m+} + k_{m-}$ is the amplitude of the line not split by the magnetic field and $c = (k_{m+} - k_{m-})/k_m$. The first term in (2) is the paramagnetic MCD and the second one is the diamagnetic effect. The integral paramagnetic magneto-optical activity (MOA) is determined by the equation:

$$c = \frac{\langle \Delta k(\omega) \rangle_0}{\langle k(\omega) \rangle_0} = C\frac{\mu_B H}{k_B(T - T_C)} \quad (3)$$

Here C is a dimensionless parameter of the MOA, k_B is the Boltzmann constant, T_C is the Curie–Weiss constant. In (3) it is supposed that, according to Van Vleck and Hebb [36], the MOA is proportional to the paramagnetic susceptibility and that both of them follow the Curie–Weiss law. The Eq. (3) is valid both for a single line and for a complex band. According to Eq. (2), the diamagnetic effect gives zero as a result of integration over the absorption band. In this part of the paper we will pay attention to the paramagnetic MCD.

The zero moments of the MCD and absorption bands, the MOA of the transitions described by (3) and their temperature dependences were found from the experimental MCD and α-absorption spectra of the crystals. As mentioned above, the temperature dependence of the paramagnetic susceptibility of the studied crystals substantially deviates from the Curie–Weiss law [11–13]. In this case it should be written

$$c = CA\chi(T) \quad (4)$$

where $\chi(T)$ is the paramagnetic susceptibility in the C_3 axis direction and A is a scale parameter. At high temperatures the paramagnetic susceptibilities of the crystals follow the Curie–Weiss law and at these temperatures Eqs. (3) and (4) should coincide. Taking this into account and introducing correction according to the real dependence $\chi(T)$, we have found parameter "C" of MOA of f–f transitions at all temperatures from the experimental temperature dependences of the parameter "c". The dimentionless parameter C of the MOA in (4) should be independent of temperature, if the MOA of the transition is proportional to the paramagnetic susceptibility. In contrast to said above, the parameter "C" appeared to be temperature dependent (Fig. 6a–g). The MOA (C) of some transitions not only depend on temperature, but even change sign with the temperature variation (Fig. 6a, c, f, and g). The studied crystals have identical (huntite-like) structure and close crystal sell parameters (Table 1), however, the MOA of the same f–f transitions in these crystals substantially

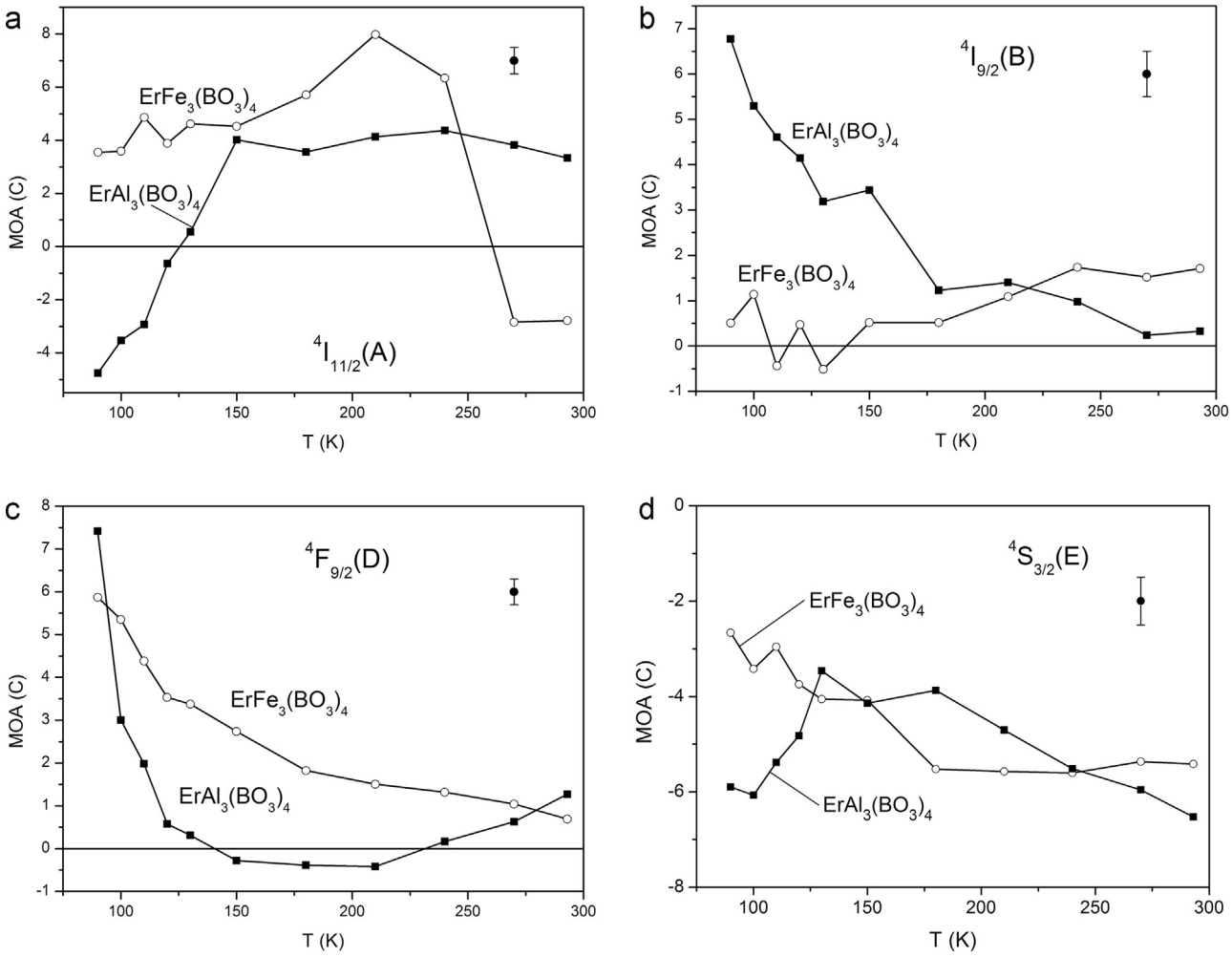

Fig. 6. (a–f) MOA of *f–f* transitions in $ErAl_3(BO_3)_4$ and $ErFe_3(BO_3)_4$. Excited states are shown in figures. (g) MOA of *f–f* transitions in $ErAl_3(BO_3)_4$. Excited states are shown in the figure.

differ (Fig. 6a–f).

It is well known, that the MOA of allowed transitions follows the Van Vleck and Hebb theory [36], i. e., the MOA is proportional to the magnetic susceptibility. Additionally, the MOA of allowed transitions is practically independent of the crystal structure. The presented above experimental results have shown that both of these statements are not fulfilled for the forbidden *f–f* transitions. These phenomena require explanation. They were considered early in detail in Ref. [24]. Briefly situation is the following.

For the *f–f* transitions to be allowed, the states with the opposite parity should be admixed to 4*f*-states (to the excited 4*f*-states in a first approximation) by the static or dynamic odd components of the crystal field (CF). The admixed J'_F state should satisfy the selection rule:

$$\left|J'_F - J_I\right| \le 1 \tag{5}$$

where J_I is the total angular-momentum of the ground state. In particular, the *f–f* transitions from the $J_I = 15/2$ ($^4I_{15/2}$) ground state of the Er^{3+} ion can become allowed due to an admixture of states with $J = 13/2$, 15/2 and 17/2 to the excited 4*f* states. The Judd–Ofelt theory gives the additional selection rule for the parity forbidden *f–f* transitions, allowed by odd components of the CF [37]:

$$\left|J_F - J_I\right| \le l \tag{6}$$

Here J_F is the total angular-momentum of the excited state and $l = 2$, 4 and 6 for the 4*f* shell. All considered excited states of Er^{3+} ion satisfy this condition at least at one value of the parameter *l*. From Eqs. (5) and (6) it is evident that the admixed states should satisfy also the following condition:

$$\left|J_F - J'_F\right| \le l - 1 \tag{7}$$

Allowed transitions from the ground state to the admixed states provide both the absorption intensity and the MOA of the *f–f* transition. The MOA of the mentioned allowed transitions in free atom was found in Ref. [24]:

$$\begin{aligned} &\text{for the transition } J \to (J-1)\text{: } C = -g(J+1)/2,\\ &\text{for the transition } J \to J\text{: } C = -g/2,\\ &\text{for the transition } J \to (J+1)\text{: } C = +gJ/2. \end{aligned} \tag{8}$$

For the ground state $^4I_{15/2}$ of Er^{3+} ion the Landé factor $g = 1.2$. Then we find possible MOA (*C*) of *f–f* transitions in Er^{3+} ion: –5.1, –0.6, and 4.5, corresponding to admixtures of states $J = 13/2$, 15/2 and 17/2, respectively. If all components of the crystal field split ground state are almost equally populated, the results (8) are valid for the integral over the *f–f* absorption band paramagnetic MOA (*C*) in crystals. In Table 2 the experimental MOA (*C*) are given at highest (room) temperature, when the condition of the population of the ground state sublevels is better fulfilled. It is seen from Table 2 that the maximum observed MOA of *f–f* transitions are close to the theoretical ones. If we compare the experimental data of Table 2 with the theoretical values, we can conclude, what of

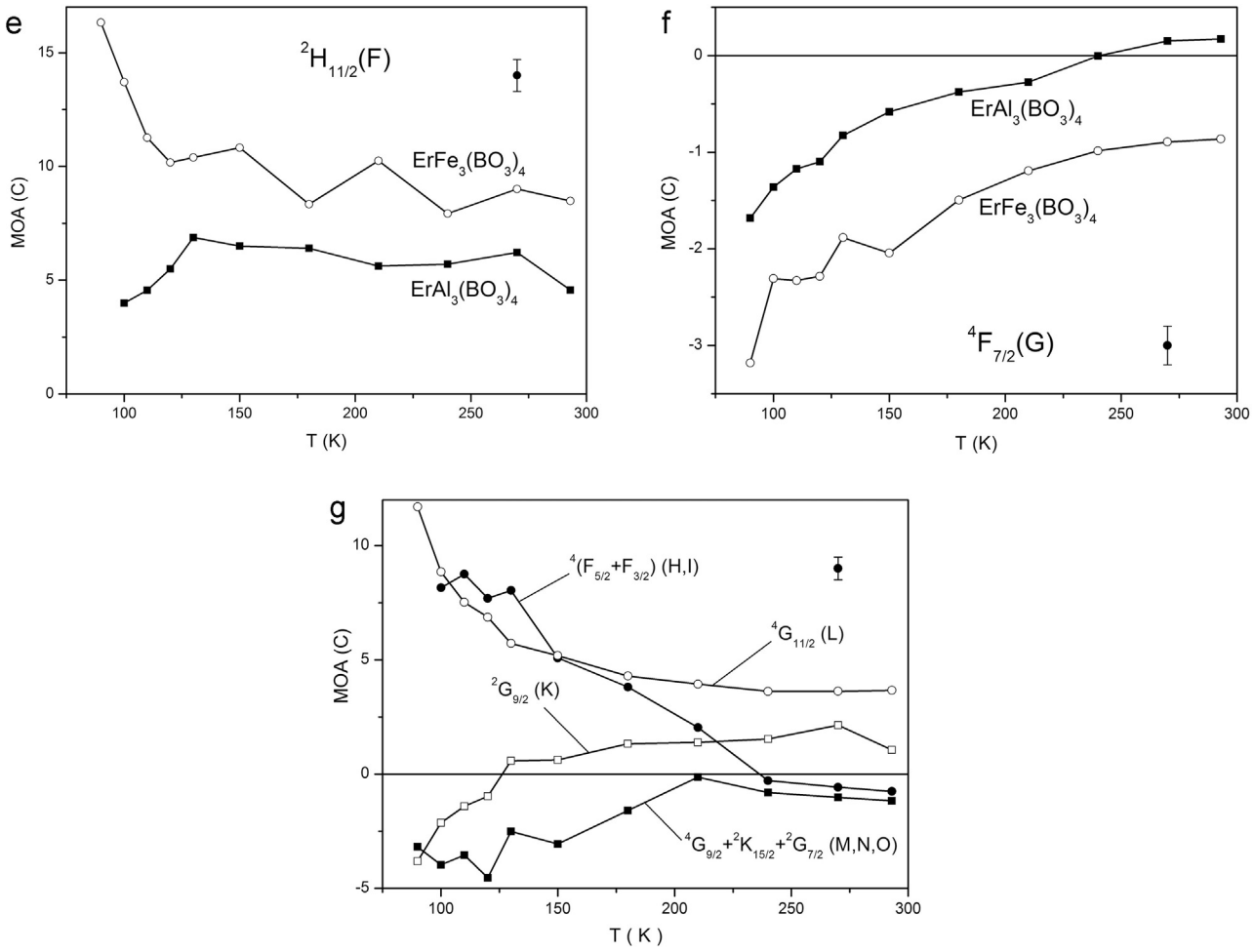

Fig. 6. (*continued*)

Table 1
a and *c* are parameters of the crystal sells, Er–O is the distance between Er ion and nearest oxygen ions, α is angle between bottoms of the triangle prism of oxygen ions, counted from the centrosymmetrical state of the prism.

Crystal	a (Å)	*c* (Å)	Er–O (Å)	α (deg)	Reference
$ErFe_3(BO_3)_4$	9.566(4)	7.591(3)	2.380 (3)	47	[10]
$ErAl_3(BO_3)_4$	9.2833(7)	7.2234(6)	2.318 (2)	44	[9]

Table 2
Integral paramagnetic MOA of *f–f* absorption bands.

Symbol	Excited state	*C* ($ErAl_3(BO_3)_4$)	*C* ($ErFe_3(BO_3)_4$)
A	$^4I_{11/2}$	2.1	−2.8
B	$^4I_{9/2}$	0.7	1.6
D	$^4F_{9/2}$	1.28	0.7
E	$^4S_{3/2}$	−6.5	−5.4
F	$^2H_{11/2}$	4.6	8.5
G	$^4F_{7/2}$	0.17	−0.86
H,I	$^4F_{5/2}+^4F_{3/2}$	−0.72	
K	$^2G_{9/2}$	1.1	
L	$^4G_{11/2}$	3.66	
M,N,O	$^4G_{9/2}+^2K_{15/2}+^2G_{7/2}$	−1.2	

the admixtures allows the concrete *f–f* transition and creates its MCD. The possibility of variants can result in the different MOA of the same *f–f* transition in different compounds. Indeed, in spite of the close parameters of the lattice sells of the studied crystals (Table 1), the MOA of the same *f–f* transitions are substantially different and even signs of the MOA are different in some cases (Fig. 6 and Table 2). This means that the odd distortions of the local environment of the Er^{3+} ion both in the ground and in the excited states in the considered crystals are different. In particular, the parameter α in Table 1 characterizes deviation of the Er^{3+} ion environment from the centrosymmetrical one. Therefore mainly this parameter influences the intensity of *f–f* transitions. The MOA of *f–f* transitions is much more sensitive to the local environment of the RE ion than the intensity of absorption is, since the contributions into the MOA have different signs, while contributions into the intensity of *f–f* transitions are of the same sign.

As said above, the Eq. (8) are well applied to *f–f* transitions, if all sublevels of the crystal field splitting of the ground state are almost equally populated, but this condition is usually not fulfilled for rare earth ions. In particular, the total CF splitting of the Er^{3+} ion ground state in the $Er:YAl_3(BO3)_4$ crystal is 316 cm^{-1} (455 K) [38]. Then, the ratio of the contributions (8) into the MOA can change with the temperature variation. If several contributions occur, this results in the deviation of the MOA temperature dependence from that of the paramagnetic susceptibility. Indeed, the best correspondence to the paramagnetic susceptibility dependence ($C \approx$ const) is observed for E and F bands in the $ErAl_3(BO_3)_4$ (Figs. 6d and 6e) and for E band in the $ErFe_3(BO_3)_4$ (Fig. 6d), when the parameter *C* at room temperature (Table 2) is close to one of the possible theoretical values. Some deviations of *C* from the constant can be partially connected with the experimental error. The temperature dependence of the A-band MOA is certainly not a smooth function (Fig. 6a). This can testify to the temperature

dependent local distortions at the temperature of the singularity in the corresponding excited state.

All considered excited states of Er^{3+} ion satisfy the condition (7) at least at one value of the parameter l and with at least one admixed state. Comparing the experimental (Table 2) and the theoretical MOA of the transitions, we conclude that the transition $\rightarrow {}^2H_{11/2}$ (F-band) in the $ErAl_3(BO_3)_4$ and $ErFe_3(BO_3)_4$ is allowed only by the admixture of the state $J=17/2$ to the excited state, while transition $\rightarrow {}^4S_{3/2}$ (E-band) is allowed by the admixture of the $J=13/2$ state. From Eq. (7) it follows that for the transition $\rightarrow {}^6S_{3/2}$ (E) it is the only admixture which can allow the transition. It corresponds to $l=6$ and to spherical harmonics $t = l \pm 1$ in the CF expansion [37].

3.2. Natural circular dichroism

As mentioned above, the natural circular dichroism (NCD) can exist if the crystal structure has no centre of inversion, and the NCD was really observed in the $ErAl_3(BO_3)_4$ crystal (Fig. 3). The presence of the NCD means also that inverse twins of one type prevail. The fine structure of the MCD spectra is conditioned by the splitting of absorption lines in the magnetic field, but the fine structure of the NCD spectra is conditioned by the splitting in the crystal field. Therefore the NCD spectra qualitatively repeat the absorption spectra, but with different signs. The integral natural optical activity (NOA) of a transition is defined by the formula:

$$A = \frac{R_{if}}{D_{if}} \approx \frac{\langle \Delta k \rangle_0}{\langle k \rangle_0} \tag{9}$$

where k is the coefficient of absorption and Δk is the NCD. Both of them are measured in α-polarization. The NOA, evidently, has no the magnetic susceptibility as a factor. The integral intensities of the NCD and absorption bands were found from the NCD and absorption spectra. As a result, the temperature dependences of the NOA (A) were obtained (Fig. 7a–c).

According to Ref. [39]:

$$R_{if} = \mathrm{Im}[\langle i|\vec{d}|f\rangle\langle f|\vec{m}|i\rangle] \tag{10}$$

where $\vec{d}$ and $\vec{m}$ are the electric and magnetic dipole moments, respectively. $D_{if} = |\langle i|\vec{d}|f\rangle|^2$, since considered transitions are mainly of the electric dipole nature. Due to the presence of the magnetic dipole matrix element in (10), the selection rules for the NCD differ from those for the electric dipole transitions. The space dispersion is the necessary phenomenological condition of the NOA existence in a substance: $A \sim s/\lambda$, where s is the size of the object absorbing light and λ is the light wave length. But this is not enough condition: the NOA exists only in the noncentro-symmetrical compounds and should be proportional to the deviation of the active cluster from the centro-symmetrical one: $A \sim \delta$, where δ is some parameter, characterizing this deviation. Thus:

$$A \sim s\delta/\lambda \tag{11}$$

According to (10), the nonzero probability of the transition in the magnetic dipole approximation is the one more necessary condition for the NCD existence. Taking into account spin–orbit interaction, all considered transitions are magnetic dipole allowed. The NOA of allowed transitions does not depend on temperature, if

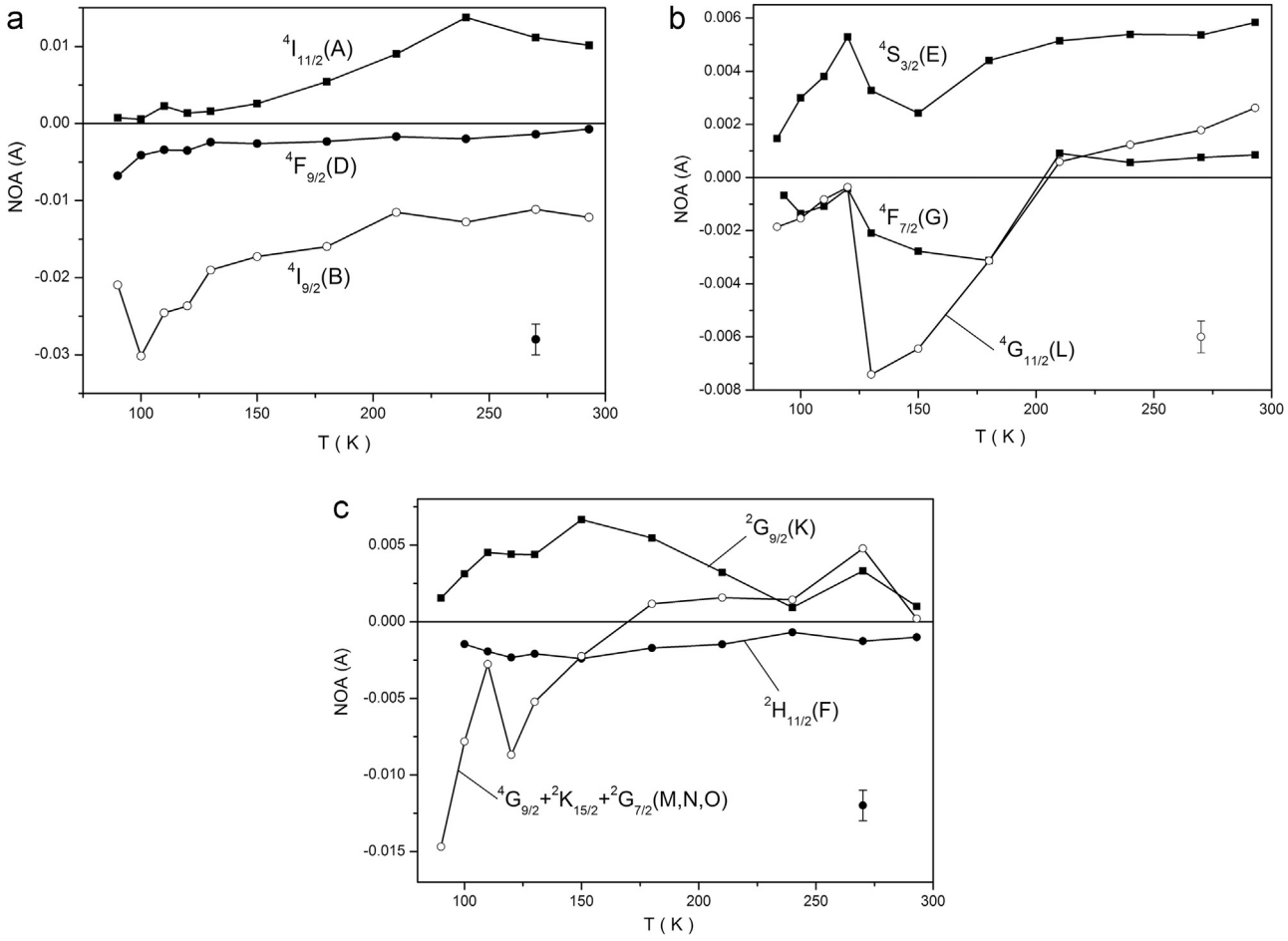

Fig. 7. (a–c) NCD of f–f transitions in $ErAl_3(BO_3)_4$. Excited states are shown in figures.

degree of the noncentro-symmetry (δ) does not change with the temperature.

The integral NOA of *f–f* transitions, the same as the MOA and absorption, should contain three contributions, corresponding to three admixed functions of opposite parity which allow the *f–f* transition in the electric dipole approximation. The same as in the case of the MOA, these contributions can have different signs and their ratio also can depend on temperature. However, the temperature dependence of this ratio differs from that for the MOA and results in the different temperature dependences of the NOA and MOA (compare Figs. 6 and 7 for $ErAl_3(BO_3)_4$). Additionally, the temperature dependences of the MOA and NOA depend on the temperature variations of the local environment geometry. The temperature dependence of the ratio of the contributions into the MOA and NOA should result in the smooth functions of them on temperature. The singularities in the MOA and NOA temperature dependences of some transitions (Figs. 6 and 7), testify to the local distortions in the corresponding excited states. If the distortions were in the ground state, then the singularities would be identical on the temperature dependences of all transitions. If there is only one contribution into the *f–f* transition allowance, then the temperature dependence of the NOA reflects only the temperature variation of the nearest environment in the excited state. According to said in the discussion of the MOA, these are the E and F bands (see also the NOA in Figs.7b and 7c). It is also worth noting that the temperature dependences of the NOA of the transitions into the quartet states are qualitatively similar (Fig. 7b).

3.3. $^4i_{15/2} \rightarrow {}^4s_{3/2}$ transition

It is worth considering this transition separately. We shall begin with the $ErAl_3(BO_3)_4$ crystal. The linearly polarized spectra of the transition are presented in Fig. 8. The MCD and NCD spectra together with the α-polarized absorption spectrum are depicted in Fig. 9. The excited state $^4S_{3/2}$ is split into the states $E_{1/2}$ and $E_{3/2}$ in the D_3 local symmetry. According to the selection rules of Table 3, the observed linear polarizations π, σ and σ of the transitions E1 and E2, respectively (Fig. 8, Table 4), from the lowest level of the ground state testify that the lowest level has $E_{1/2}$ symmetry and the levels E1 and E2 have the $E_{1/2}$ and $E_{3/2}$ symmetries, respectively. The lines E1a, E2a and E1b were identified as transitions from the next states of the ground state crystal field splitting (Fig. 10), taking into account their linear polarizations.

Electron states of atoms in crystals with the axis of symmetry

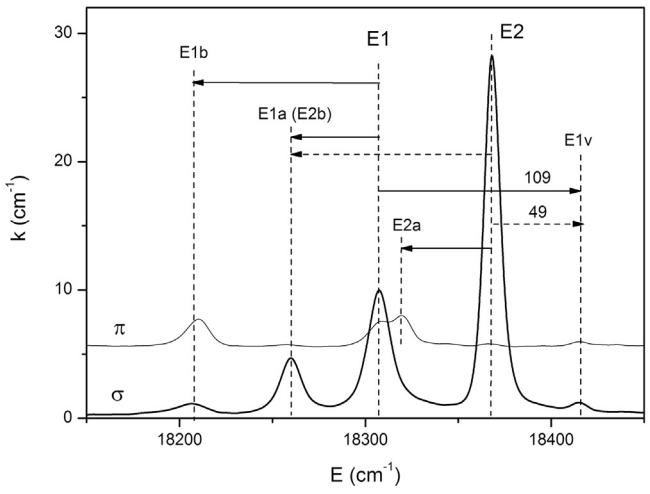

Fig. 8. Polarized absorption spectra of $^4I_{15/2} \rightarrow {}^4S_{3/2}$ transition (E band) in $ErAl_3(BO_3)_4$ at $T=90$ K.

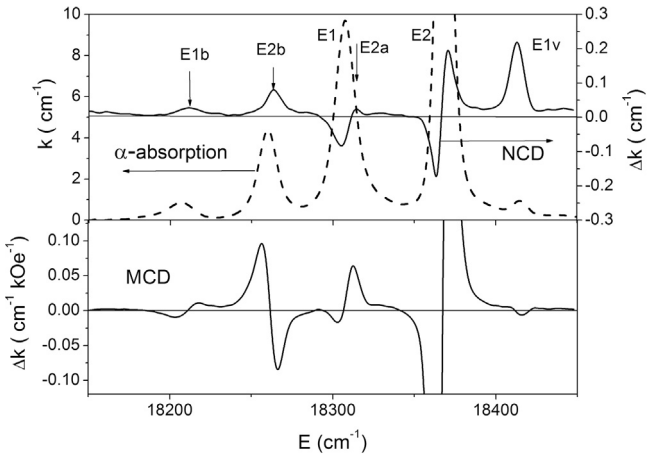

Fig. 9. α-polarized absorption spectrum, MCD spectrum and NCD spectrum of $^4I_{15/2} \rightarrow {}^4S_{3/2}$ transition (E band) in $ErAl_3(BO_3)_4$ at $T=90$ K.

Table 3
Selection rules for electric dipole transitions in D_3 symmetry.

	$E_{1/2}$	$E_{3/2}$
$E_{1/2}$	π, $\sigma(\alpha)$	$\sigma(\alpha)$
$E_{3/2}$	$\sigma(\alpha)$	π

Table 4
Properties of transitions: $\Delta\omega_0$ is the Zeeman splitting according to (1), Δg_C (measured) is the measured change of the effective Landé factor in the C_3-direction during transition, Δg_{CM} (theory) is the theoretical change of the effective Landé factor in the C_3-direction during transition in the $|J, \pm M_J\rangle$ functions approximation, NCD (A) is the natural circular dichroism according to (9).

Transition	E1	E2	E1a	E2a	E1b	E2b	E1v
Polarization	π, σ	σ	σ	π	π, σ	(σ)	π, σ
sign of $\Delta\omega_0$ (measured)	plus	plus	minus		plus	(minus)	minus
sign of $\Delta\omega_0$(theory)	minus	plus	minus		plus	minus	
Δg_C (measured)		+8.4	−9.9			(-9.9)	
Δg_{CM} (theory)	−17.6	+9.6	−16		+11.2	−19.2	
NCD (A)	−0.01	~0	+0.018	+	+0.02	(+0.018)	+0.4

are characterized by the crystal quantum number μ. In the case of the C_3 axis and the half integer total moment J of the atom, there are three possible values of the crystal quantum number [40]: $\mu = +1/2, -1/2, 3/2\ (\pm 3/2)$. In the trigonal symmetry, the states with $M_J = \mu \pm 3n$ (where $n=0, 1, 2, \ldots$) correspond to each μ [40], where M_J is the projection of the atom total moment. As a result, the following set of states takes place in the considered crystals:

$$\begin{aligned} M_J &= \pm 1/2, \pm 3/2, \pm 5/2, \pm 7/2, \pm 9/2, \pm 11/2, \\ &\quad \pm 13/2, \pm 15/2 \\ \mu &= \pm 1/2, (\pm 3/2), \mp 1/2, \pm 1/2, (\pm 3/2), \\ &\quad \mp 1/2, \pm 1/2, (\pm 3/2) \end{aligned} \tag{12}$$

The states $E_{1/2}$ correspond to $\mu = \pm 1/2$ and the states $E_{3/2}$ correspond to $\mu = (\pm 3/2)$. The selection rules for the crystal quantum number μ in the case of electric dipole absorption are the following [39]:

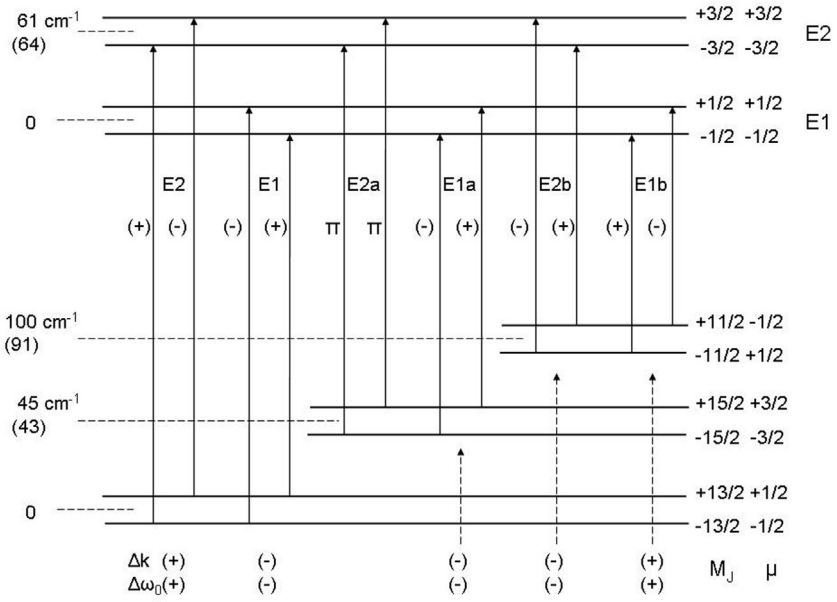

Fig. 10. Diagram of $^4I_{15/2} \rightarrow {}^4S_{3/2}$ transition (E band). Energies in brackets correspond to $ErFe_3(BO_3)_4$.

$\Delta\mu = \pm 1$ corresponds to $\mp$ circularly polarized and
σ–polarized waves,

$\Delta\mu = 0$ corresponds to π–polarized waves. (13)

For linearly polarized waves these selection rules coincide with that of Table 3.

In the axially symmetric crystal field, the electron wave functions can be described in a first approximation by the $|J, \pm M_J\rangle$ states. The diamagnetic part of the MCD can help to identify the crystal field states in the $|J, \pm M_J\rangle$ presentation and to find the Zeeman splitting of these states. The Zeeman splitting of an absorption line $2\Delta\omega_0$ is determined by the Zeeman splitting of the initial and final states [24]:

$$2\hbar\Delta\omega_0 = \pm\left(\Delta E_i \pm \Delta E_f\right) \quad (14)$$

The first sign in (14) coincides with the sign of the paramagnetic MCD (c in Eq. (2)) which corresponds to polarization of the transition from the lower component of the Zeeman splitting of the initial state. The second sign in (14) shows that the splitting of states can sum up and subtract. This is so, since the polarization of transitions is governed by the crystal quantum number μ according to (13) and (12), but the Zeeman splitting is governed in a first approximation by the value of M_J. With the help of (12) and (13) and taking into account that in a first approximation the splitting of the Kramers doublets in magnetic field is proportional to $\pm M_J$, the diagram of transitions and their polarizations in magnetic field directed along the C_3 axis has been created (see Fig. 10).

Apropos. If the intensity of transitions from the lower components of the ground state crystal field splitting prevails in the total absorption of the band, then the integral paramagnetic MOA can be substantially larger than that predicted by (8) (see Table 2). Indeed, according to [24] the MOA of transitions from the state $|J, M_J = J\rangle$ are about twice as large as those given in (8).

For the MCD written in the form (1), in Ref. [24] it was shown that, if signs of $\partial k/\partial\omega$ and $\Delta k(\omega)$ coincide, the diamagnetic effect $\Delta\omega_0$ is negative and vice versa. Thus we find signs of the diamagnetic effects of the transitions from the experimental MCD spectrum of Fig. 9 (Table 4). Majority of them coincide with the theoretical ones predicted with the help of Eq. (14) and the diagram of Fig. 10. If absorption and MCD spectra of transitions are good resolved, it is possible to find values of the Zeeman splitting $\Delta\omega_0$ from the absorption and MCD spectra. According to [24] for the Lorentz shape of the absorption line (as in our case) it is:

$$\Delta\omega_0 = 2\frac{\Delta k_{dm}}{k_m}\left|\omega_m - \omega_0\right| \quad (15)$$

Here Δk_{dm} and ω_m are the value and position of extremums of the diamagnetic MCD of the line, respectively, and k_m is amplitude of the α-absorption of the line. The splitting of the Kramers doublets in the magnetic field directed along the C_3 axis of a crystal is given in the form: $\Delta E = \mu_B g_C H$, where g_C is the effective Landé factor in the C_3-direction. Therefore, for the transitions between the Kramers doublets

$$2\hbar\Delta\omega_0 = \mu_B H \Delta g_C \quad (16)$$

Here Δg_C is the difference of the effective Landé factors g_C of states taking part in the transition. They were found for the E2 and E1a lines (see Table 4). Signs of Δg_C correspond to signs of $\Delta\omega_0$.

It is possible to estimate the effective Landé factors of the Kramers doublets along the C_3 axis, g_{CM}, in the $|J, \pm M_J\rangle$ functions approximation. In Ref. [24] it was shown that $g_{CM} = 2gM_J$, where g is the Landé factor of the free atom. The values of g_{CM} for all doublets of the ground and excited multiplets of the Er^{3+} ion are given in Table 5. Now, taking into account (16), (14) and Fig. 10, it is possible to find values of Δg_{CM} in approximation of the $|J, \pm M_J\rangle$ functions (Table 4). For the E2 and E1a lines they are a little larger in absolute values than the experimental ones. It is a consequence of the mixing of functions (12) with the different M_J and equal μ in the crystal field. The E1a line could be identified also as the E2b line according to its energy (Fig. 8) and sign of the MCD (Fig. 9 and Table 4). However the theoretical Δg_{CM} for this transition differs

Table 5
Landé factors, g_{CM}, of the Kramers doublets along C_3 axis of a crystal in the approximation of $|J, \pm M_J\rangle$ states.

	M	15/2	13/2	11/2	9/2	7/2	5/2	3/2	1/2
$^4I_{15/2}$, $g=1.2$	g_{CM}	18	15.6	13.2	10.8	8.4	6	3.6	1.2
$^4S_{3/2}$, $g=2$	g_{CM}							6	2

stronger from the measured one than for the E1a transition (Table 4).

The absorption line E1v (Figs. 8, 9) is, apparently, a vibronic one. In RE ferroborates and alumoborates the A_2 and E symmetry vibrations with participation of the RE ion were found [41, 42] (81 and 105 cm^{-1}, respectively, in $YbAl_3(BO_3)_4$ [42]). These vibrations create the following vibronic states with the considered excited electronic states of the $E_{1/2}$ and $E_{3/2}$ symmetry:

$$E_{1/2} \times A_2 = E_{1/2},\ E_{1/2} \times E = E_{1/2} + E_{3/2},$$
$$E_{3/2} \times A_2 = E_{3/2},\ E_{3/2} \times E = E_{1/2} + E_{1/2}. \quad (17)$$

The E1v line has π,σ-polarization (Fig. 8). Then, according to the selection rules (Table 3) and taking into account the $E_{1/2}$ symmetry of the ground state, we conclude that the vibronic state has the $E_{1/2}$ symmetry. According to (17) such vibronic satellite of the $E_{1/2}$ (E1) state can be created both by A_2 and E vibrations, while that of the $E_{3/2}$ (E2) state only by the E vibration. In the latter case the energy of the vibration of 49 cm^{-1}, found from the absorption spectrum (see Fig. 8), is too small as compared with 105 cm^{-1} found in Ref. [42] for this vibration. Consequently, the E1v line is the vibronic satellite of the E1 line created by the E-vibration, which has the energy of 105 cm^{-1} in $YbAl_3(BO_3)_4$ [42]. In our case energy of the vibration is 109 cm^{-1}.

The NOA (A) of the separate lines at 90 K are presented in Table 4. The absolute values of the NOA of the separate electronic lines are about one order of magnitude larger than the integral NOA of the whole E-band at the same temperature (Fig. 7b). The NOA of the vibronic line E1v is more than one order of magnitude larger than that of the electronic lines (Table 4). This is quite natural. Indeed, the vibronic wave function is much more delocalized than the purely electronic one. Therefore, according to (11), the NCD should be much larger.

The NCD in the region of the E2 line demonstrates the splitting of this line and, consequently, of the E2 state (Fig. 9). Using the described above procedure, we have found this splitting to be: $2\Delta\omega_0 = 0.11$ cm^{-1}. (For comparison, the Zeeman splitting of the same line in $H = 1$ kOe is: $2\Delta\omega_0 = 0.39$ cm^{-1}.) As mentioned above, the NCD and MCD were measured simultaneously. In order to exclude possible influence of the magnetic field, the measurement of the NCD was also fulfilled separately without the magnetic field. The result was the same. This splitting is observed up to room temperature. The splitting of the Kramers doublet in the crystal field is impossible. Consequently, the observed phenomenon means that there are two kinds of the absorbing centers.

The linearly polarized spectra of the discussed transition in the $ErFe_3(BO_3)_4$ are presented in Fig. 11. The MCD spectrum and the α-polarized absorption spectrum are depicted in Fig. 12. The NCD in this crystal is on the level of noise. The identification of states (see Fig. 11) was done by analogy with the $ErAl_3(BO_3)_4$ spectra. The spectra of the $ErFe_3(BO_3)_4$ have a number of features as compared with the $ErAl_3(BO_3)_4$ spectra. The vibronic line E1v in the $ErFe_3(BO_3)_4$ is much stronger than in the $ErAl_3(BO_3)_4$ (compare Figs. 9 and 11) and it corresponds to the vibration of 103 cm^{-1}. The E2 and E2a lines are observed both in π and σ polarizations, while in the $ErAl_3(BO_3)_4$ they are purely σ and π polarized, respectively, in agreement with the D_3 local symmetry. This testifies to decrease of the local symmetry in the $ErFe_3(BO_3)_4$. It is known that in some rare earth ferroborates the phase transition to the $P3_121$ space symmetry (C_2 local symmetry of Er^{3+} ion) occurs with the decreasing temperature [43]. Information about the phase transition in the $ErFe_3(BO_3)_4$ is rather indefinite [13, 41]. Therefore we have undertaken measurements of the heat capacity in this crystal.

The results of the studying of the anomalous part of the heat capacity of the $ErFe_3(BO_3)_4$ crystalline sample upon heating are

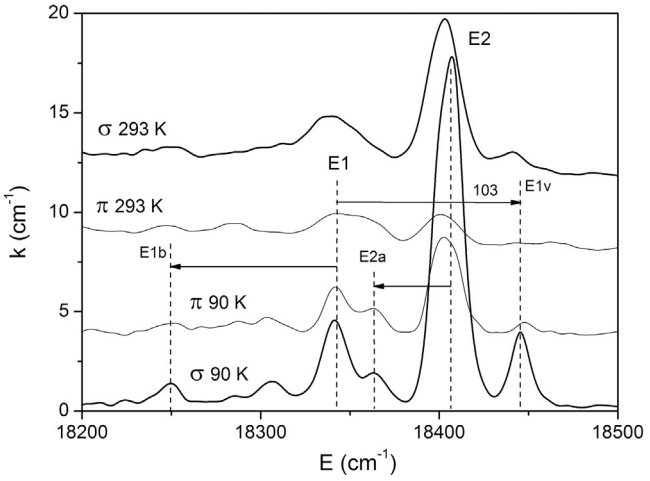

Fig. 11. Polarized absorption spectra of $^4I_{15/2} \rightarrow {}^4S_{3/2}$ transition (E band) in $ErFe_3(BO_3)_4$ at two temperatures.

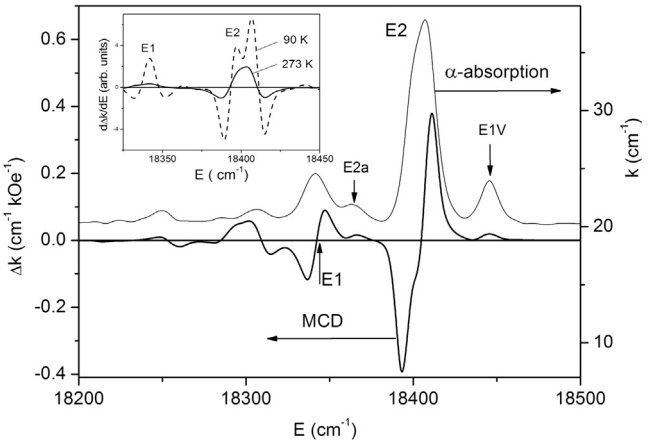

Fig. 12. α-polarized absorption spectrum and MCD spectrum of $^4I_{15/2} \rightarrow {}^4S_{3/2}$ transition (E band) in $ErFe_3(BO_3)_4$ at $T = 90$ K. Inset: derivatives of the $ErFe_3(BO_3)_4$ MCD spectra at two temperatures.

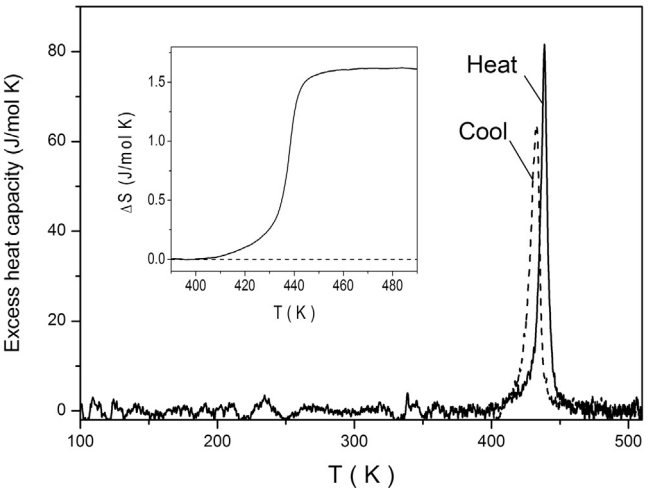

Fig. 13. Temperature dependences of the excess heat capacity and the excess entropy ΔS (inset) measured in the heating and in the cooling modes.

presented in Fig. 13. The temperature dependence of the excess heat capacity was calculated after extraction of the lattice heat capacity C_{lat} which was approximated by a smooth polynomial function. The good agreement was found between the calculated C_{lat} and the experimental data outside the heat capacity abnormal

behavior. In the heating mode, the anomaly of the heat capacity ΔC_p at $T=439\pm1$ K was observed. The measurements carried out also in the cooling mode revealed the anomaly of ΔC_p at $T=433\pm1$ K (dotted line in Fig. 13). So the corresponding temperature hysteresis was about 6 K that approves the first-order phase transition.

The integral thermodynamic characteristics associated with the phase transition were obtained by processing the calorimetric results. The excess enthalpy is characterized by the following value: $\Delta H=\int\Delta C_p(T)dT=(700\pm70)$ J/mol. The entropy ΔS corresponding to the anomalous behavior of the heat capacity was calculated by the integrating of the function $(\Delta C_p/T)(T)$ and was shown in Fig. 13, inset. The small value of the excess entropy $\Delta S=1.6$ J/mol K $\approx 0.2\ R$ points to the displacive type of the phase transition. Thus, indeed, at all temperatures of the optical measurements the $ErFe_3(BO_3)_4$ crystal has the space symmetry lower than the $R32$ one (presumably $P3_121$) and the local symmetry lower than the D_3 (presumably C_2).

In contrast to the $ErAl_3(BO_3)_4$ crystal, the natural splitting of the E2 line in the $ErFe_3(BO_3)_4$ is so large ($11.3\ cm^{-1}$) that it is seen directly on the absorption and MCD spectra at $T=90$ K (Fig. 12). At room temperature it is not seen directly, but it is seen on the spectrum of the MCD derivative (Fig. 12, inset), which corresponds to the second derivative of the absorption spectrum according to Eq. (2).

The discussed splitting is observed only on the single transition. This means that it is the local phenomenon connected with the definite excited electron state. The components of the E2 line splitting have the natural circular dichroism of opposite signs (Fig. 9), i. e., the Er^{3+} centers are somehow connected with the opposite twins. The opposite helicoids of AlO_6 octahedrons refer to the opposite twins. The helicoidal chains are equivalent in the $ErAl_3(BO_3)_4$ crystal in the ground electron state, but they can be locally nonequivalent in the excited state. The helicoidal chains of FeO_6 octahedrons in the $ErFe_3(BO_3)_4$, which has lower symmetry, are nonequivalent in the ground electron state [44], and the discussed splitting in this crystal is much larger. Consequently, the nonequivalence of the helicoidal chains also has an attitude to the observed phenomenon.

4. Summary

The absorption and magnetic circular dichroism spectra of the $ErFe_3(BO_3)_4$ and $ErAl_3(BO_3)_4$ single crystals were measured as a function of temperature in the range of 90–293 K. In the same temperature range the natural circular dichroism spectra of $ErAl_3(BO_3)_4$ were measured. On the basis of these data, the temperature dependences of the paramagnetic MOA and of the NOA of f–f transitions were obtained. It was found out that the MOA of the same transitions in the studied crystals substantially differed and their temperature dependences did not follow the Curie–Weiss law in contrast to the properties of allowed transitions. The observed phenomena are due to the existence of at least three contributions into the f–f transition allowance and of the corresponding contributions into the MCD with the different signs. In some temperature dependences of the MOA and NOA the singularities were revealed which indicated to some local structural distortions in the corresponding excited states.

Properties of the transition $^4I_{15/2}\rightarrow{}^4S_{3/2}$ were studied in detail. In particular, the Zeeman splitting and the NOA of the separate absorption lines were determined. The vibronic line with the very large natural optical activity was revealed in both studied crystals. The origin of this line was identified as being due to the repetition of the $E_{1/2}\rightarrow E_{1/2}$ electron transition by the E symmetry vibration. Two nonequivalent Er^{3+} ion positions were revealed in the $ErAl_3(BO_3)_4$ crystal in one of the excited states. The first of them can be referred to the equivalent inverse twins and the second one: to the boundaries between the twins. Similar positions were identified in the $ErFe_3(BO_3)_4$ as well. In this crystal, where symmetry is lower and the helicoidal chains are nonequivalent in the ground electron state, the corresponding splitting of the absorption line is much larger than in the alumoborate. However, it is observed also only in the same excited state of the Er^{3+} ion.

Polarization properties of the $^4I_{15/2}\rightarrow{}^4S_{3/2}$ transition in the $ErFe_3(BO_3)_4$ have shown that the local symmetry of the Er^{3+} ion in this crystal is lower than the D_3 one in the range of 90–293 K. From the heat capacity measurements it was found out, that the first order structural phase transition to lower symmetry occurred in the $ErFe_3(BO_3)_4$ at 433–439 K.

Acknowledgments

The work was supported by the Russian Foundation for Basic Researches Grant 12-02-00026 and by the President of Russia Grant no. Nsh-2886.2014.2.

References

[1] Y.J. Chen, Y.F. Lin, X.H. Gong, Q.G. Tan, Z.D. Luo, Y.D. Huang, Appl. Phys. Lett. 89 (2006) 241111.
[2] N.I. Leonyuk, V.V. Maltsev, E.A. Volkova, O.V. Pilipenko, E.V. Koporulina, V. E. Kisel, N.A. Tolstik, S.V. Kurilchik, N.V. Kuleshov, Opt. Mater. 30 (2007) 161.
[3] Y. Chen, Y. Lin, X. Gong, J. Huang, Z. Luo, Y. Huang, Opt. Lett. 37 (2012) 1565.
[4] P. Dekker, J.M. Dawes, J.A. Piper, Y.G. Liu, J.Y. Wang, Opt. Commun. 195 (2001) 431.
[5] E. Cavalli, A. Speghini, M. Bettinelli, M.O. Ramirez, J.J. Romero, L.E. Bausa, J. G. Sole, J. Lumin. 102 (2003) 216.
[6] M. Rico, M.C. Pujol, F. Díaz, C. Zaldo, Appl. Phys. B 72 (2001) 157.
[7] R.A. McFarlane, Appl. Phys. Lett. 54 (1989) 2301.
[8] J.Y. Allain, M. Monerie, H. Poignant, Electron. Lett. 28 (1992) 111.
[9] A.V. Malakhovskii, T.V. Kutsak, A.L. Sukhachev, A.S. Aleksandrovsky, A. S. Krylov, I.A. Gudim, M.S. Molokeev, Chem. Phys. 428 (2014) 137.
[10] A.V. Malakhovskii, V.V. Sokolov, A.L. Sukhachev, A.S. Aleksandrovsky, I. A. Gudim, M.S. Molokeev, Phys. Solid State 56 (2014) 2056, Fizika Tverdogo Tela 56 (2014) 1991.
[11] K.-C. Liang, R.P. Chaudhury, B. Lorenz, Y.Y. Sun, L.N. Bezmaternykh, I.A. Gudim, V.L. Temerov, C.W. Chu, J. Phys.: Conf. Ser. 400 (2012) 032046.
[12] E.A. Popova, A.N. Vasiliev, V.L. Temerov, L.N. Bezmaternykh, N. Tristan, R. Klingeler, B. Büchner, J. Phys.: Condens. Matter 22 (2010) 116006.
[13] C. Ritter, A. Vorotynov, A. Pankrats, G. Petrakovskii, V. Temerov, I. Gudim, R. Szymczak., J. Phys.: Condens. Matter 22 (2010) 206002.
[14] A.M. Kadomtseva, Yu. F. Popov, G.P. Vorob'ev, A.P. Pyatakov, S.S. Krotov, K. I. Kamilov, V. Yu. Ivanov, A.A. Mukhlin, A.K. Zvezdin, A.M. Kuz'menko, L. N. Bezmaternykh, I.A. Gudim, V.L. Temerov, Low Temp. Phys. 36 (2010) 511 ФНТ 36, 640 (2010).
[15] M.N. Popova, E.P. Chukalina, T.N. Stanislavchuk, L.N. Bezmaternykh, J. Magn. Magn. Mater. 300 (2006) e440.
[16] E.A. Popova, A.N. Vasiliev, V.L. Temerov, L.N. Bezmaternykh, N. Tristan, R. Klingeler, B. Büchner., J. Phys.: Condens. Matter 22 (2010) 116006.
[17] C. Ritter, A. Vorotynov, A. Pankrats, G. Petrakovskii, V. Temerov, I. Gudim, R. Szymczak., J. Phys.: Condens. Matter 22 (2010) 206002.
[18] S.J. Collocott, K.N.R. Taylor, J. Phys. C: Solid State Phys. 11 (1978) 2885.
[19] U.V. Valiev, A.A. Klochkov, A.S. Moskvin, P. Shiroki, Opt. Spektrosk. 69 (1990) 111, Opt. Spectrosc. 69 (1990) 68.
[20] A.A. Klochkov, U.V. Valiev, A.S. Moskvin, Phys. Status Solidi B 167 (1991) 337.
[21] D.P. Poulios, D.E. Johnson, N.P. Bigelow, J.P. Spoonhower, J. Non-Cryst. Solids 239 (1998) 181.
[22] P.G. Feldmann, H. Le Gall, M. Guillot, IEEE Trans. Magn. 21 (1985) 1669.
[23] G. Corradi, Th Lingner, A.B. Kutsenko, V. Dierolf, K. Polgar, J.-M. Spaeth, W. Von der Osten, Radiat. Eff. Defects Solids 155 (2001) 223.
[24] A.V. Malakhovskii, A.L. Sukhachev, A. Yu., Strokova, I.A. Gudim, Phys. Rev. B 88 (2013) 075103.
[25] L. Alyabyeva, V. Burkov, O. Lysenko, B. Mill, Opt. Mater. 34 (2012) 803.
[26] V.I. Burkov, O.A. Lysenko, B.V. Mill, Crystallogr. Rep. 55 (2010) 983.
[27] K.A. Schoene, J.R. Quagliano, F.S. Richardson, Inorg. Chem. 30 (1991) 3803.
[28] V.I. Burkov, A.V. Egorysheva, A.Y. Vasil'ev, Y.F. Kargin, V.M. Skorikov, Inorg. Mater. 38 (2002) 1035.
[29] L. Fluyt, I. Couwenberg, H. Lambaerts, K. Binnemans, C. Görller-Walrand, J. Chem. Phys. 105 (1996) 6117.
[30] I.A. Gudim, E.V. Eremin, V.L. Temerov, J. Cryst. Growth 312 (2010) 2427.
[31] K. Teshima, Y. Kikuchi, T. Suzuki, S. Oishi, Cryst. Growth Des. 6 (2006) 1766.
[32] I. Couwenberg, K. Binnemans, H. De Leebeeck, C. Görller-Walrand, J. Alloy.

Compd. 274 (1998) 157.
[33] A.V. Malakhovskii, S.L. Gnatchenko, I.S. Kachur, V.G. Piryatinskaya, A. L. Sukhachev, I.A. Gudim, J. Alloy. Compd. 542 (2012) 157.
[34] A.A. Kaminskii, Crystalline Lasers: Physical Processes and Operating Schemes, CRC Press, New York/London/Tokyo, 1996.
[35] A.V. Malakhovskii, A.L. Sukhachev, A.D. Vasil'ev, A.A. Leont'ev, A.V. Kartashev, V.L. Temerov, I.A. Gudim, Nature of optical properties of $GdFe_3(BO_3)_4$ and $GdFe_{2.1}Ga_{0.9}(BO_3)_4$ crystals and other $3d^5$ antiferromagnets, Eur. Phys. J. B 85 (2012) 80.
[36] J.H. Van Vleck, M.H. Hebb, Phys. Rev. 46 (1934) 17.
[37] R.D. Peacock, Struct. Bond. 22 (1975) 83.
[38] A. Baraldi, R. Capelletti, N. Magnani, M. Mazzera, E. Beregi, I. Földvári, J. Phys.: Condens. Matter 17 (2005) 6245.
[39] W. Moffit, A. Moscovitz, J. Chem. Phys. 30 (1959) 648.
[40] M.A. El'yashevitch, Spectra of rear earths, Moskow, 1953 (in Russian).
[41] D. Fausti, A.A. Nugroho, P.H.M. van Loosdrecht, S.A. Klimin, M.N. Popova, L. N. Bezmaternykh, Phys. Rev. B 74 (2006) 024403.
[42] K.N. Boldirev, B.N. Mavrin, M.N. Popova, L.N. Bezmaternykh, Opt. Spectrosc. 111 (2011) 420.
[43] Y. Hinatsu, Y. Doi, K. Ito, M. Wakeshima, A. Alemib, J. Solid State Chem. 172 (2003) 438.
[44] S.A. Klimin, D. Fausti, A. Meetsma, L.N. Bezmaternykh, P.H.M. van Loosdrecht, T.T.M. Palstra, Acta Crystallogr. B 61 (2005) 481.